2021 IEEE 18th International Symposium on Biomedical Imaging (ISBI)
April 13-16, 2021, Nice, France

PARTICLE-BASED SEGMENTATION OF EXTENDED OBJECTS ON CURVED BIOLOGICAL MEMBRANES

A. Solomatina[1,2,3] *Y. Kalaidzidis*[2,5] *A. Cezanne*[2] *K. Soans*[2,4,6] *C. Norden*[2,6]
M. Zerial[2,3,4] *I. F. Sbalzarini*[1,2,3,4]

[1] Technische Universität Dresden, Faculty of Computer Science, Dresden, Germany
[2]Max Planck Institute of Molecular Cell Biology and Genetics, Dresden, Germany
[3]Center for Systems Biology Dresden, Dresden, Germany
[4]Cluster of Excellence Physics of Life, TU Dresden, Dresden, Germany
[5]Moscow State University, Faculty of Bioengineering and Bioinformatics, Moscow, Russia
[6]Instituto Gulbenkian de Ciência (IGC), Oeiras, Portugal

ABSTRACT

We present a novel method for model-based segmentation of extended, blob-like objects on curved surfaces. Our method addresses several challenges arising when imaging curved biological membrane, such as out-of-membrane signal and geometry-induced background variations. We use a particle-based reconstruction of the membrane geometry, moment-conserving intensity interpolation from pixels to surface particles, and model-based in-surface segmentation. Our method denoises and deconvolves images, corrects for background variations, and quantifies the number, size, and intensity of segmented objects. We benchmark the accuracy of the method and present two applications to (1) neuroepithelial focal adhesion sites during optic cup morphogenesis in zebrafish and (2) reconstituted membrane domains bearing the small GTPase Rab5 on spherical beads.

***Index Terms*—** Fluorescence microscopy, membrane imaging, model-based segmentation, mesh-particle interpolation, curved surfaces

1. INTRODUCTION

Membranes are of central importance for a variety of biological processes. The key players in membranes—lipids and proteins—are known to compartmentalize laterally and organize into blob-like spatial domains or patterns on the membrane that often are prerequisite to molecular function [1]. Quantification of these patterns is challenging when membranes form curved surfaces. Imaging them produces 3D volumetric data from which the 2D manifold needs to be reconstructed. In fluorescence microscopy, the prevalent modality for live imaging, this reconstruction is hampered by out-of-membrane signal and curvature-induced intensity variations, caused by the anisotropic point spread function (PSF) of the microscope.

These spurious effects need to be corrected for when reconstructing the membrane from the 3D image and segmenting objects intrinsic to the membrane. In previous works, domain size on curved membranes was analyzed by thresholding along 1D lines around axially symmetric shapes not affected by imaging artifacts [2]. A popular method for spherical membranes is based on projecting the intensity from the sphere into two hemispheres [3]. While such approaches work in individual applications, they are not generic to arbitrary curved surfaces.

Here, we propose a method to quantify and segment domains on curved membranes of any shape, imaged by volumetric fluorescence microscopy, such as light-sheet or confocal microscopy. Our method exploits the 2D nature of membranes to reduce memory and computational costs. However, unlike previous approaches [4], our method is not limited to star-convex closed manifolds. Instead, we use a narrow-band particle representation of arbitrarily shaped curved manifolds, as inspired by particle level-set methods [5], and exploit intensity-moment conserving mesh-to-particle interpolation [6] to map intensity values from the 3D pixel grid to the particles representing the surface. Therefore, our pipeline conserves total intensity and the center of intensity mass.

Besides intensity moment conservation, the particle representation also simplifies physically correct normal projections and deconvolving model-based in-surface segmentation. We benchmark the accuracy of this approach using synthetic images, compare with manual segmentations, and estimate the error of object size quantification as a function of the signal-to-noise ratio (SNR) of the images. Finally, we demonstrate the practical application of our pipeline to adhesion sites of migrating neuroepithelial cells during optic cup morphogenesis in zebrafish and to reconstituted domains consisting of the small GTPase Rab5 on lipid-coated beads, showcasing two distinct biological applications that share similar methodological challenges.

978-0-7381-2593-0/21/$31.00 ©2021 IEEE

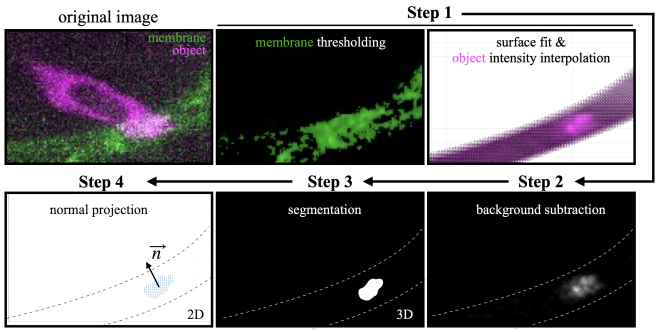

Fig. 1. Illustration of the four steps of the present method for intrinsic object segmentation on curved membranes (example image: migrating neuroepithelial cell). See main text for details.

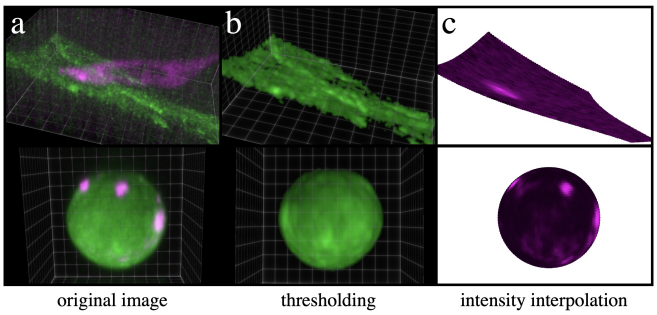

Fig. 2. Surface extraction and intensity interpolation: The signal of the membrane (a) is thresholded (b) and used to fit a geometric surface model. Then, the surface is represented by a narrow band of particles, and the intensity of the imaged objects is interpolated from the original image pixels to the surface particles (c). Top row: example from the neuroepithelial dataset; bottom row: example from the Rab5 dataset.

2. METHOD

We present a particle-based segmentation pipeline to quantify the number, size, and intensity of extended objects on curved membranes imaged by volumetric fluorescence microscopy. The pipeline consists of the following steps, as illustrated in Fig. 1 and described in detail in the following sub-sections:

1. Membrane surface extraction and pixel-to-particle intensity interpolation.
2. Background subtraction in tangent space [7].
3. Segmentation of domains using deconvolving segmentation [8].
4. Normal projection of the segmented structures onto the 2D manifold and size estimation.

2.1. Surface extraction and pixel-to-particle interpolation

The membrane is detected and extracted from a separate color channel containing a specific membrane label. This provides a relatively homogeneous signal on the membrane, which is used for geometry processing. We start by applying a 3×3 median filter to reduce shot noise, followed by selecting all pixels in the upper 0.5% intensity percentile. This should result in a subset of (but not necessarily all) pixels that belong to the membrane surface (see Fig. 2a,b). These pixels are then used to fit a parametric 2D surface model. In general, we fit the surface by cubic polynomial splines. If prior knowledge about the surface geometry is available, such as for spherical membrane beads, this can be used here. For spherical beads, we fit the sphere center and radius. Fitting is done using a linear least-squares solver for the unknown coefficients of the shape model with the normal residual as cost function. After fitting the 2D surface model, we distribute particles on the fitted surface to generate a discrete particle representation of the surface. Particles are placed on a regular Cartesian grid in x–y with z coordinates from the geometric surface model. On a sphere, particles are placed on a latitude-longitude mesh with 3° resolution in both azimuthal and polar directions. In order to account for imaging diffraction and out-of-focus signal, the particles are subsequently extended from the surface into a narrow band around it. This is done by replicating each particle along the local surface normal with 1 pixel spacing until a distance of 5 pixel from the surface. This results in a narrow-band representation of the curved surface, as is classic in level-set methods [5].

Image intensity values from the raw object channel (i.e., not thresholded) are interpolated from the pixels to the particles. This amounts to representing the object channel intensity as a particle function approximation [9]. Interpolation from the surrounding pixels onto the narrow-band particles is done using moment-conserving interpolation schemes [6]. This yields the intensity $I(\mathbf{x}_p)$ of particle p at continuous position $\mathbf{x}_p = (x_p, y_p, z_p)$ as:

$$I(\mathbf{x}_p) = \sum_{q=1}^{L} \tilde{I}(\mathbf{x}_q) W\left(\frac{x_p - x_q}{\Delta x}\right) W\left(\frac{y_p - y_q}{\Delta y}\right) W\left(\frac{z_p - z_q}{\Delta z}\right) \tag{1}$$

from the pixel intensities $\tilde{I}(\mathbf{x}_q)$ of the L neighboring pixels q at $x_q = (x_q, y_q, z_q)$. The interpolation kernel W is [6]:

$$W(s) = \begin{cases} 1 - \frac{1}{2}(5|s|^2 - 3|s|^3), & \text{if } |s| \leqslant 1 \\ \frac{1}{2}(2 - |s|)^2(1 - |s|), & \text{if } 1 < |s| \leqslant 2 \\ 0, & \text{if } |s| > 2 \end{cases} \tag{2}$$

for the normalized distance $s = (x_p - x_q)/\Delta x$, where Δx is the pixel size in x-direction (analogous for y and z). The interpolation kernel considers a neighborhood of $L = 4{\times}4{\times}4$ pixels around each particle. The kernels are independently evaluated in x, y, and z, leading to a linear computational cost of $3{\cdot}4 = 12$ evaluations instead of $4^3 = 64$. This interpolation scheme is 3^{rd} order accurate and exactly conserves the total intensity as well as the center of intensity mass, yielding a physically correct dimensionality reduction.

In order to allow for fitting errors during surface extraction and small surface undulations, the particle intensity values are maximum-projected in the direction of the local surface normal. This is done by replacing the interpolated intensity of each on-surface particle by the maximum of any particle in the narrow band along the surface normal through it. This yields a topologically generic representation of the membrane with the associated surface intensity distribution.

2.2. Background subtraction in tangent space

Imaging a curved membrane by fluorescence microscopy can cause a homogeneously labeled membrane to appear inhomogeneous in the image. The magnitude of this intensity distortion depends on the membrane curvature and on the anisotropy of the microscope PSF. We correct for this effect using a sliding window algorithm, inspired by the rolling ball algorithm, which is well known in the field of biological image processing [8, 10]. On a curved surface, a moving window represents a 2D segment of the surface that slides along the surface in tangential direction. In each window, the minimum intensity value is taken as the background estimate at the center pixel. We implement this algorithm on the particles created in the previous step. In particle representation, we iterate through the surface particles and find all particles within a spherical neighborhood, hence defining the in-surface sliding window. The neighborhood radius is defined by the user analogously to the window size in the classic rolling ball algorithm. It must be larger than the objects of interest, but smaller than the radius of curvature of the surface.

2.3. Surface domain segmentation

To segment domains or spatial patterns in the intensity channel of interest on the curved surface (see Fig. 3), we use a globally optimal model-based segmentation method that corrects for PSF blur, providing a deconvolving segmentation [11]. This is important when in-surface object sizes are close to diffraction limited, as PSF blur on thin membranes is significant. We use the globally optimal Squassh method [8], implemented in the MOSAICsuite plug-in for the bio-image processing frameworks Fiji[12] and ImageJ [13, 14].

We perform all segmentations using the following parameters in Squassh: the *regularization* parameter controlling the smoothness of the segmentation is set to 0.35. The *minimum object intensity* sets a threshold on normalized intensity below which all objects are discarded and is set to 0.3. We enable sub-pixel segmentation with 4-fold oversampling.

Squassh segmentation is applied on pixels after replacing all pixel values with intensities obtained by interpolating back from the particles to the pixels. This particle-to-pixel interpolation is done using the same moment-conserving interpolation scheme as described above. It yields a clean pixel image with denoised and background-corrected intensities only at the pixels close to the membrane. This enables using existing pixel-based 3D segmentation tools as drop-in modules.

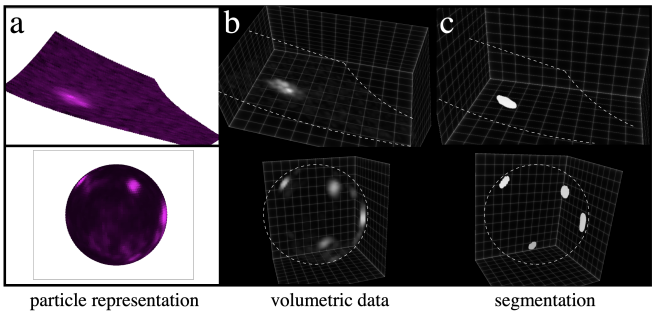

Fig. 3. Domain segmentation: Corrected particle intensities (a) are interpolated back to pixels to yield a clean volumetric image (b). Segmentation is performed in 3D on the pixels to yield surface objects (c). Top row: example from the neuroepithelial dataset; bottom row: example from the Rab5 dataset.

2.4. Normal projection of the segmentation to the surface and domain size estimation

After the segmentation has been performed in the embedding space, we project the segmented objects to the curved surface to effectively estimate 2D sizes of domains. We use a marching cubes algorithm [15] to construct a closed triangulated mesh of the surface of each segmented object [16]. The triangulated mesh is then used to map the segmentation to the particles in the narrow band. Each particle within the triangulated mesh is orthogonally projected onto the surface using surface normals defined by the fitted geometry model from Step 1. For domain size estimation, we sum areas of the surface elements corresponding to the particles belonging to a domain.

3. BENCHMARKS

We benchmark the robustness and accuracy of our method using synthetic images of beads of 10 μm (=100 pixel) diameter with predetermined circular domains of varying radii 0.5...1.5 μm and intensities representing different SNR. We generate the benchmark images as follows: we place spheres with surface intensity $O(\mathbf{x})$ onto a constant background of intensity B. Then, we convolve the scene with the measured PSF $K(\mathbf{x})$ of the microscope and add modulatory Poisson noise to the result. This yields an image $I(\mathbf{x}) = \mathbf{P}(K(\mathbf{x}) * (O(\mathbf{x}) + B))$, where $\mathbf{P}(\lambda)$ is a Poisson-distributed random variable with mean λ and $*$ denotes a discrete convolution with 5-fold oversampling. For Poisson noise, the SNR is [17]:

$$\mathrm{SNR} = \frac{\max(O(\mathbf{x})) - B}{\sqrt{\max(O(\mathbf{x}))}}. \quad (3)$$

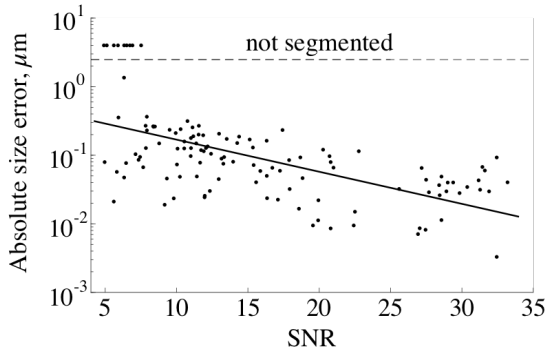

Fig. 4. Absolute error in segmented domain radius evaluated in synthetic images of different SNR. The dashed line shows the Rayleigh resolution limit. The solid line is a linear fit to the 120 data points.

We generate images of size $111 \times 111 \times 48$ pixel at different SNR by varying the foreground intensity O at constant $B = 250$ for 16-bit intensity values. The SNR is computed locally for each domain, and the segmentation error is defined as the absolute difference between the reconstructed radius of a domain and its true radius. Figure 4 shows the results for 120 domains of different sizes at different SNR along with a linear trend line. As expected, the error decreases with increasing SNR. The dashed line indicates the Rayleigh resolution limit of the microscope. The domains on the spheres were segmented with super-resolution precision and with errors of the same order for different true radii. Nine out of the 120 domains were not segmented at all; all of these false negatives were for SNR < 8 (symbols above the dashed line,"not segmented"). Processing one image took 162 s of computer time on a quad-core 2.2 GHz Intel Core i7 with 16 GB RAM.

4. APPLICATIONS

We showcase the application of our pipeline by quantifying the focal adhesion sites of migrating neuroepithelial cells during optic cup morphogenesis in zebrafish (*Danio rerio*) embryos (see Figs. 2 and 3, top row). Zebrafish embryos were imaged with an Andor Spinning disk microscope with an Andor iXon Ultra 897 monochrome EMCCD camera using an Olympus UPLSAPO 60X/1.3NA silicon-oil objective. Using the present method, we quantify the size of the adhesion site to be 13.17 μm^2. For comparison, we also perform manual segmentation in the tangent plane of each adhesion site, leading to an estimated area of 13.04 μm^2 in good agreement with the result of the proposed pipeline.

The second application considers biochemically reconstituted domains of GFP-tagged Rab5 GTPase on spherical lipid-coated beads (see Figs. 2 and 3, bottom row). Silica beads of 10 μm diameter were coated in a supported lipid bilayer (SLB) using a protocol adapted from [18]. The lipid-coated beads were incubated with recombinant proteins (geranylgeranylated GFP-Rab5/GDI complex, GDI and Rabex5/Rabaptin5-RFP complex) and imaged using a Nikon TiE microscope with a 100x/1.45NA Plan Apochromat DIC oil-immersion objective, a Yokogawa CSU-X1 scan head and an Andor DU-897 back-illuminated CCD camera. In total, the present method segmented 449 domains on 96 beads with a mean domain area of 1.74 μm^2. Quantifying the size of membrane domains was crucial for identifying the molecular mechanisms of self-organization by which they form [19].

5. CONCLUSION

We have presented a particle-based method to segment and quantify extended objects and domains on curved membranes. Our method exploits the 2D nature of biological membranes using a narrow-band particle function approximation. Moment-conserving interpolation maps the image intensity signal from the 3D pixel grid to the surface particles. We have described each step of the method in detail and benchmarked its accuracy using synthetic images and manual segmentation. We showcased two applications to real data from migrating neuroepithelial cells during optic cup formation in zebrafish and Rab5 domain formation reconstituted *in vitro* on complex lipid membranes.

Despite the many differences between these two applications, the present method addressed their joint methodological challenges. Segmentation quality was good in both examples, with errors below 0.1 μm (< 1 pixel) for SNR above 8, according to the presented benchmarks. Nevertheless, our method currently has several limitations. The most important one is that it will not perform well if the size of the domains to be segmented on a membrane is comparable to the overall size of the membrane. In this case, the task would better be formulated as an end-to-end optimization problem with specific shape priors for the membrane. Second, our method currently requires two-color images with a dedicated membrane channel separate from the object channel. While this is convenient, it is not strictly required, as it would be sufficient to know the membrane geometry in the immediate vicinity of the objects to be segmented. Third, we use rather classic and simplistic methods for surface extraction (linear least squares) and background removal (rolling ball). We did so in order to demonstrate that they are sufficient to yield good results in conjunction with the particle-based surface representation. However, they can be replaced by more sophisticated methods if required.

Despite these limitations, the method presented here is applicable to a range of problems, as illustrated by the two distinct showcases. It is easy to implement and modular. We therefore believe that particle representation of arbitrarily shaped surfaces and moment-conserving pixel-to-particle interpolation can be useful in a variety of situations, also beyond the specific applications considered here.

6. COMPLIANCE WITH ETHICAL STANDARDS

This is a computational image-analysis pipeline for which no ethical approval was required.

7. ACKNOWLEDGMENTS

No external funding was received to conduct this study. The authors have no relevant financial or non-financial interests to disclose.

8. REFERENCES

[1] B. Sönnichsen, S. De Renzis, E. Nielsen, J. Rietdorf, and M. Zerial, "Distinct membrane domains on endosomes in the recycling pathway visualized by multicolor imaging of Rab4, Rab5, and Rab11," *Journal of Cell Biology*, vol. 149, no. 4, pp. 901–914, 2000.

[2] N. W. Goehring, P. K. Trong, J. S. Bois, D. Chowdhury, E. M. Nicola, A. A. Hyman, and S. W. Grill, "Polarization of PAR proteins by advective triggering of a pattern-forming system," *Science*, vol. 334, no. 6059, pp. 1137–1141, 2011.

[3] E. S. Fried, Y.-M. Li, and M. L. Gilchrist, "Phase composition control in microsphere-supported biomembrane systems," *Langmuir*, vol. 33, no. 12, pp. 3028–3039, 2017.

[4] B. Schmid, G. Shah, N. Scherf, M. Weber, K. Thierbach, C. P. Campos, I. Roeder, P. Aanstad, and J. Huisken, "High-speed panoramic light-sheet microscopy reveals global endodermal cell dynamics," *Nature Communications*, vol. 4, no. 1, pp. 2207, 2013.

[5] S. E. Hieber and P. Koumoutsakos, "A Lagrangian particle level set method," *Journal of Computational Physics*, vol. 210, pp. 342–367, 2005.

[6] J. J. Monaghan, "Extrapolating B splines for interpolation," *Journal of Computational Physics*, vol. 60, no. 2, pp. 253–262, 1985.

[7] S. R. Sternberg, "Biomedical image processing," *Computer*, vol. 16, no. 1, pp. 22–34, 1983.

[8] A. Rizk, G. Paul, P. Incardona, M. Bugarski, M. Mansouri, A. Niemann, U. Ziegler, P. Berger, and I. F. Sbalzarini, "Segmentation and quantification of subcellular structures in fluorescence microscopy images using Squassh," *Nature Protocols*, vol. 9, pp. 586–596, 2014.

[9] G.-H. Cottet and P. Koumoutsakos, *Vortex methods – Theory and Practice*, Cambridge University Press, 2000.

[10] B. K. Huang, S. Ali, K. T. Stein, and H. D. Sikes, "Interpreting heterogeneity in response of cells expressing a fluorescent hydrogen peroxide biosensor," *Biophysical Journal*, vol. 109, no. 10, pp. 2148–2158, 2015.

[11] J. A. Helmuth and I. F. Sbalzarini, "Deconvolving active contours for fluorescence microscopy images," in *Proc. Intl. Symp. Visual Computing (ISVC)*, Las Vegas, USA, 2009, vol. 5875 of *Lecture Notes in Computer Science*, pp. 544–553, Springer.

[12] J. Schindelin, I. Arganda-Carreras, E. Frise, V. Kaynig, M. Longair, T. Pietzsch, S. Preibisch, C. Rueden, S. Saalfeld, B. Schmid, J.-Y. Tinevez, D. J. White, V. Hartenstein, K. Eliceiri, P. Tomancak, and A. Cardona, "Fiji: an open-source platform for biological-image analysis," *Nature Methods*, vol. 9, pp. 676–682, 2012.

[13] M. Abramoff, P. Magalhães, and S.J. Ram, "Image processing with ImageJ," *Biophotonics International*, vol. 11, pp. 36–42, 2003.

[14] C.A. Schneider, W.S. Rasband, and K.W. Eliceiri, "NIH Image to ImageJ: 25 years of image analysis," *Nature Methods*, vol. 9, pp. 671–675, 2012.

[15] W.E. Lorensen and H.E. Cline, "Marching cubes: A high resolution 3D surface construction algorithm," *SIGGRAPH Computer Graphics*, vol. 21, no. 4, pp. 163–169, 1987.

[16] P. Hammer, "MATLAB implementation of marching cubes," https://www.mathworks.com/matlabcentral/fileexchange/32506-marching-cubes, 2020, Accessed: 2020-10-01.

[17] I. F. Sbalzarini and P. Koumoutsakos, "Feature point tracking and trajectory analysis for video imaging in cell biology," *Journal of Structural Biology*, vol. 151, no. 2, pp. 182–195, 2005.

[18] S. Neumann, T. J. Pucadyil, and S. L. Schmid, "Analyzing membrane remodeling and fission using supported bilayers with excess membrane reservoir.," *Nature Protocols*, vol. 8, no. 1, pp. 213–222, 2013.

[19] A. Cezanne, J. Lauer, A. Solomatina, I. F. Sbalzarini, and M. Zerial, "A non-linear system patterns Rab5 GTPase on the membrane," *eLife*, vol. 9, pp. e54434, 2020.